Nanoscale

PAPER

View Article Online
View Journal | View Issue

Cite this: *Nanoscale*, 2022, **14**, 5404

AC-assisted deposition of aggregate free silica films with vertical pore structure†

Gilles E. Moehl, *[a] Tauqir Nasir, [a] Yisong Han,[b] Yasir J. Noori, [c] Ruomeng Huang, [c] Richard Beanland, [b] Philip N. Bartlett [a] and Andrew L. Hector *[a]

Received 15th December 2021,
Accepted 15th March 2022

DOI: 10.1039/d1nr08253a

rsc.li/nanoscale

Silica thin films with vertical nanopores are useful to control access to electrode surfaces and may act as templates for growth of nanomaterials. The most effective method to produce these films, electrochemically assisted surfactant assembly, also produces aggregates of silica particles. This paper shows that growth with an AC signal superimposed onto the potential avoids the aggregates and only very small numbers of single particles are found. This finding is linked to better control of the diffusion field of hydroxide ions that are responsible for particle growth. The resultant films are smooth, with very well-ordered hexagonal pore structures.

Introduction

Mesoporous silica films have a wide range of applications in sensing devices, as biomaterials and as functional coatings.[1–4] A widely used method to deposit such films is evaporation induced self-assembly (EISA), which relies on the evaporation of a solvent driving the sol–gel transition of a solution containing a surfactant.[5,6] The surfactant assembles during the process and leads to the formation of highly ordered thin films. When 1-dimensional channels are produced with this technique, the pores tend to align parallel to the substrate.[7] Efforts have been made to establish routes resulting in vertically aligned (*i.e.* perpendicular to the substrate) pores,[8] one of the most effective of which is the electrochemically assisted self-assembly (EASA) method. This technique is comparable to electrodeposition approaches to make porous metal films.[9–11] Pioneered by Walcarius *et al.*, it requires the application of a cathodic potential to an electrode immersed in a surfactant-containing silica sol. A typical sol consists of tetraethyl orthosilicate (TEOS), cetrimonium bromide (CTAB) and the supporting electrolyte $NaNO_3$ in a 1 : 1 EtOH/H_2O mixture at pH = 3.[12] The sol is prepared with acidic pH (pH = 3), as this condition favours precursor hydrolysis over condensation, inhibiting the premature formation of a silica gel. This behaviour is reversed under alkaline conditions – the basis of the EASA process: the electrochemically induced change of local pH from acidic to alkaline enhances the condensation of pre-hydrolysed precursor species around the cationic surfactant, resulting in the growth of a silica film with hexagonally packed channels in a direction normal to the electrode surface. Thin films have been shown to form on a variety of conductive materials (glassy carbon, ITO, Au, TiN).[12–16] Typical thicknesses of the compact film (without any aggregates) are around 100 nm,[13] although a wider range of obtainable film thicknesses would be advantageous to access higher aspect ratios.

The EASA process produces aggregates of spherical particles stuck to the surface of the aligned mesoporous films, through the operation of the standard Stöber process in basic solution.[17] The number of these aggregates increases with deposition time and hence constrains the achievable film thickness. The formation of particle aggregates is not avoidable with the regular EASA experimental procedure, as it is the natural result of applying a potential to drive hydroxide generation, which in turn leads to the bulk condensation of the silica precursor as the hydroxide diffuses into the layer close to the electrode surface. The expansion of the pH gradient takes place within very short time and on a large scale compared to the thickness of the mesoporous silica film, so significant bulk reaction is observed even when using short deposition times. The sol composition can be refined to minimise aggregates, but any change, *e.g.* a reduction of the precursor concentration, will always affect both parts of the process.

In recently published work, Vanheusden *et al.* have shown that aggregate formation can be suppressed in favour of increased film thickness through the use of a rotating disk electrode.[18] The concept was to minimise the thickness of the

[a]*School of Chemistry, University of Southampton, SO17 1BJ, UK. E-mail: A.L.Hector@soton.ac.uk, G.E.H.K.Moehl@soton.ac.uk*
[b]*Department of Physics, University of Warwick, CV4 7AL, UK*
[c]*School of Electronics and Computer Science, University of Southampton, SO17 1BJ, UK*

†Electronic supplementary information (ESI) available. See https://doi.org/10.1039/d1nr08253a

reactive layer in the vicinity of the electrode without lowering the precursor concentration, while employing the rotating disk to disperse the layer of reactive species at the electrode. Previously, thicker films had been achieved through the repeated application of the EASA process to the same substrate, with rinsing steps in between depositions to remove the generated hydroxide.[19,20]

In this work, we deposit aggregate-free mesoporous silica films using a novel EASA process in which a sinusoidal potential is applied, oscillating between values at which hydroxide generation is high and low. This results in a modulated hydroxide flux at the working electrode surface. Thus, the hydroxide concentration gradient at the electrode divides into an oscillating region and a static gradient of much lower strength.[21] This favours the formation of the compact film at the electrode surface while generating significantly fewer surface particles. Secondly, the nitrate-based supporting electrolyte was left out of the sol composition to reduce the hydroxide ion flux and hence slow down the rate of condensation.[22,23] The achievable ordered film thickness increases considerably, making higher aspect ratios of the pore channels available.

Results and discussion

Our silica films were deposited by applying a sinusoidal potential, oscillating between −1 V and −2 V, at a frequency of 100 Hz. This was done in a silica sol, containing only silica precursor and surfactant in a 1 : 1 EtOH/H_2O mixture at pH = 3 (see "Experimental" for details). The optical appearance of the silica films immediately after deposition was distinctively different from those deposited using the usual constant potential method, as strong iridescence was exhibited in reflected light. This indicates the presence of a much smoother film surface. The effect was most prominent for samples deposited at 15 000 and 20 000 oscillation periods, while the sample made with 30 000 periods had a more turbid appearance, indicating increased scattering. Samples made using the same nitrate-free solution and regular constant potential conditions showed either thick white aggregate layers or no film at all and were not further characterised.

SEM images of the samples can be seen in Fig. 1. Images (i) and (ii) correspond to 10 000 periods, (iii) and (iv) to 15 000, (v) and (vi) to 20 000 and (vii) and (viii) to 30 000 periods of potential. The odd numbers correspond to top-down images, while the even ones indicate cross sections. It can be seen in Fig. 1(i) that very few individual spherical particles are present on the surface of the film. Their number density increases slightly with an increasing number of periods (from estimated 0.076 ± 0.008 particles per μm^2 at 10 000 periods to 0.290 ± 0.03 particles per μm^2), but under DC conditions a deposition of 300 s would produce a film covered in a thick layer of aggregates of the spherical particles. Particle sizes of the spherical particles increase from an average of 385 nm at 10 000 periods to almost double the diameter at 40 000 periods, as shown in Table S1.† From the cross sections, the thickness of the deposited films was estimated, as plotted in Fig. S1.† The film thickness increases from almost 150 nm at 10 000 periods in close to linear fashion to 350 nm at 30 000 periods, which is significantly thicker than is possible using the original route.

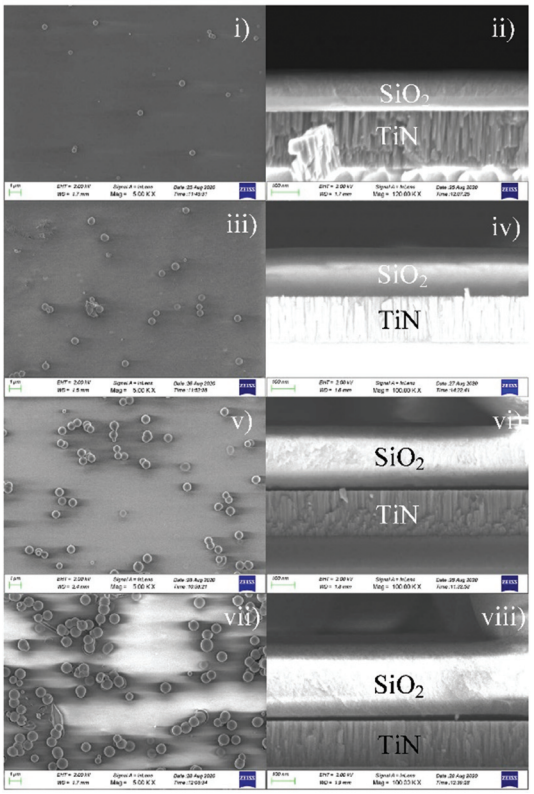

Fig. 1 SEM images of mesoporous silica films deposited at 100 Hz, between −1.0 V and −2.0 V with deposition times of 10 000 periods (i and ii), 15 000 periods (iii and iv), 20 000 periods (v and vi) and 30 000 periods (vii and viii) of potential. The left-hand images are top-down and the right-hand cross-sections on cleaved samples.

The current resulting from the application of the AC signal at 100 Hz frequency is shown in Fig. 2(a), where the inset illustrates the oscillating current in the earliest part of the deposition. The current profiles were Fourier transformed using a custom Python script, as depicted in Fig. 2(b). Once again, the inset shows a magnified part, underlining the presence of a sharp peak at 100 Hz and a definitive DC component towards low frequencies. The interesting part of the signal for this experiment is the DC component, which corresponds to the static diffusion gradient generated by the oscillating potential. Another custom Python script was used to filter out the AC component of the signal around 100 Hz by applying a band stop notch filter with a Q factor of 30. Fig. 2(c) shows the resulting current profiles with removed oscillation. These are of roughly the same order of magnitude and shape throughout all samples, with their length being the main difference. In comparison to the application of constant −2.0 V for 60 s, the current magnitude is about 10 times smaller when using the sinusoidal potential (Fig. 2d). This makes sense as the alter-

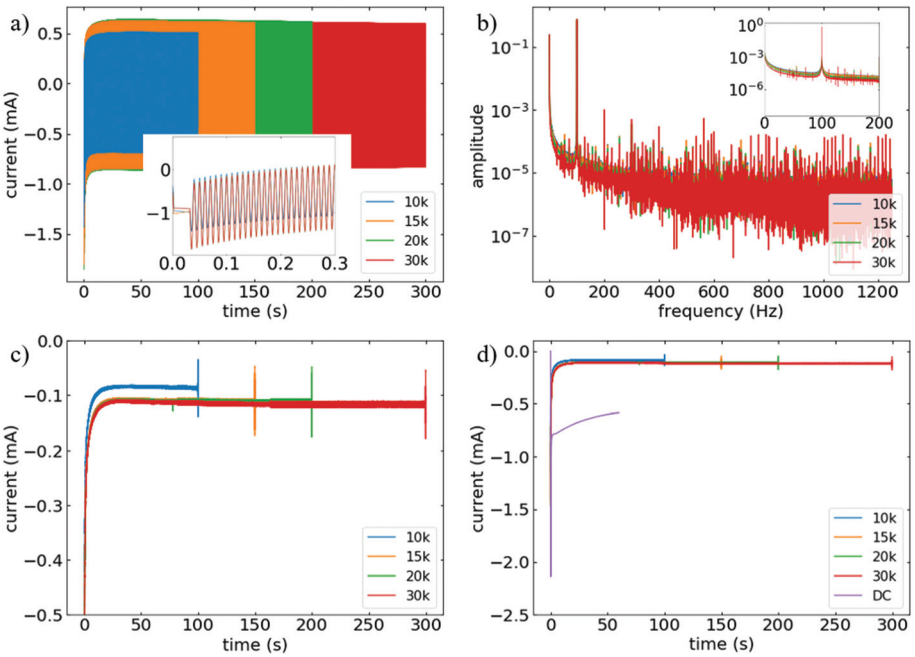

Fig. 2 (a) Raw currents recorded during the deposition of silica using a sinusoidal signal with a frequency of 100 Hz, between −1.0 V and −2.0 V with deposition times of 10 000, 15 000, 20 000, and 30 000 periods (100, 150, 200 and 300 s). Inset: zoomed plot of the same signals for the period between 0 and 0.3 s. (b) Fourier-transform of the data shown in (a) produced using a custom-made python script. Inset: zoom to the range 0–200 Hz. (c) Data from (a) filtered using another custom python script which employs a band stop notch filter at 100 Hz with Q = 30. (d) Same data as (c) plotted in conjunction with a current transient obtained from a deposition at constant potential of −2.0 V (DC) for 60 s.

nating potential mainly generates non-faradaic currents from the oscillating double layer. The "efficiency" of the signal in terms of hydroxide production at the electrode was therefore significantly decreased. The total current can be described as the sum of faradaic and capacitive currents: $j_t = j_F + j_C$, where the capacitive current depends strongly on the change of potential $\left(j_C = C\frac{d\eta}{dt}\right)$. Apart from the two peaks of the waveform, the capacitive current dominates the total current and therefore drastically decreases the generation of hydroxide at the working electrode. If one assumed the generation was most effective at the lower peak of the wave (−2 V), the process would correspond to a pulsed regime with a very short "on" time, which in turn decreases the diffusion layer thickness $\left(\delta_p = 2\sqrt{\frac{Dt_{on}}{\pi}}\right)$. This also suggests that if the frequency is increased enough, only double layer charging occurs, and no films would be deposited at all due to the total loss of faradaic current.

Grazing incidence small angle X-ray scattering (GISAXS) was used to analyse the structure and arrangement of the silica films. The images shown in Fig. 3(a–d) were measured with an incident angle of 0.3° for a duration of 15 min for the samples deposited with (a) 10 000, (b) 15 000, (c) 20 000, and (d) 30 000 periods. The four images look very similar by eye, showing horizontal spots (symmetrical *versus* q_y = 0). The GISAXS data give a representation of the film structure in reciprocal space. This means that the observed horizontal features correspond to a vertical structure in real-space.[24] The peak spacing indicates a vertically aligned two-dimensional hexagonal structure, with the two higher order peaks highlighting the high degree of ordering within the films. If the film structure was of cubic or circular nature, additional spots at higher magnitude of q_z would be expected.[25–27] The spherical particles result in a semicircle because their pore structure is not aligned, and it is noteworthy that the semicircle is very weak in all of these patterns.

The fact that this method leads to vertically aligned mesopores is quite surprising considering the common description of the EASA process. A recent review by Walcarius mentions the importance of the electric field not only for the generation of hydroxide species needed for silica condensation, but also for the templating of the surfactant at the electrode surface, resulting in vertically aligned pores.[20] Indeed, there have been studies on the behaviour of surfactants in the vicinity of electrodes, showing that the actual potential of the electrode, its surface properties (*e.g.* crystal structure) as well as the ionic strength of the environment strongly influence the shape and size of surface aggregates.[28] Thus, it appears logical to assume that when using a cationic surfactant in a silica sol, the applied potential and resulting electric field should contribute significantly to the assembly of the surfactant and the pore alignment. Indeed, it was found that only a negatively charged substrate resulted in vertically aligned silica channels in an experiment where an ultra-microelectrode was used for EASA on microdots.[29] The approach we present here amends this theory, as the oscillating electric field is constantly changing the potential landscape at the electrode. We suggest that if the

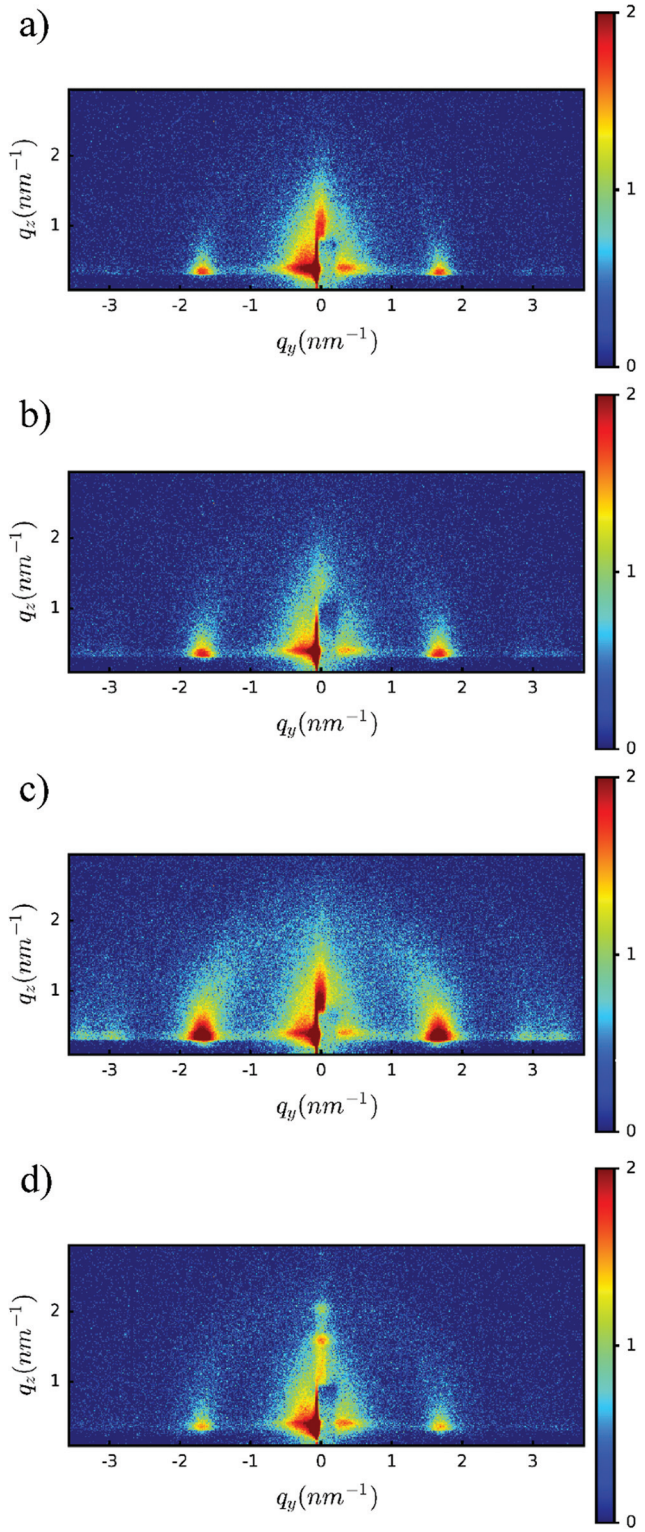

Fig. 3 2D GISAXS images measured with an incident angle of 0.3° for a duration of 15 min for mesoporous silica samples deposited at 100 Hz, between −1.0 V and −2.0 V with deposition times of (a) 10 000, (b) 15 000, (c) 20 000, and (d) 30 000 periods.

required amount of hydroxide species is provided in the form of a hydroxyl gradient decreasing from the electrode surface, silica condensation around the templated surfactant takes places independently of the momentary electrode potential. This would mean that the key factor in the process apart from the supply of hydroxide species, would be the concentration polarisation, decreasing from the electrode surface. This hypothesis is also supported by the robustness of the EASA process, which works similarly well on a variety of substrate materials.[13]

The procedure was repeated in a control experiment, where $NaNO_3$ was added to the modified sol (original sol composition typically used in constant potential deposition). The same electrochemical setup and conditions were used. After application of the sinusoidal potential, the samples were rinsed with deionised water immediately. No iridescence was visible to the naked eye for these samples – their whitish appearance hinted at the presence of numerous particle aggregates. SEM images of the films are shown in Fig. S2.† They show particle aggregates in the micron range from 15 000 periods onwards (b–d), whereby more than half of the pictured area seems to be covered at 30 000 periods. Even at only 10 000 periods (Fig. S2a†), 0.342 ± 0.04 particles per μm^2 were estimated, which is higher than the number obtained at 40 000 in the sol without $NaNO_3$. The number of particles formed during silica film deposition by the EASA process is higher when $NaNO_3$ is present in the sol, which is attributed to the higher flux of hydroxide ions. It has been suggested that $NaNO_3$ supports the formation of hydroxide at the working electrode,[12] accelerating the silica condensation process not only at the electrode surface but also in the bulk solution. As displayed in Fig. S3,† the filtered raw data of the current responses consist of a DC signal in similar range to the ones shown in Fig. 2c.

Fig. S4† displays the raw two-dimensional GISAXS images of these control samples made at (a) 10 000, (b) 15 000, (c) 20 000 and (d) 30 000 periods, measured with an incidence angle of 0.3° with an exposure time of 30 min. An increased exposure time was used for the control samples compared to the main ones (15 min) as their scattering was significantly weaker. The presence of particle aggregates is confirmed in the GISAXS data, showing strong semicircles for the samples made at 15 000, 20 000 and 30 000 periods (b–d), but not for the shortest deposition time (10 000, a). Horizontal scattering features are seen for all the control samples, whereby only the first order peak is visible. This indicates the successful formation of a vertically aligned structure below the particle aggregates, but with a much lower degree of ordering. This shows that not only the use of a sinusoidal signal, but also the exclusion of supporting electrolyte leads to the formation of higher quality films during EASA.

From the GISAXS images shown in Fig. 3 and Fig. S4,† horizontal profiles of the intensities were made by integrating intensities along q_y which are shown in Fig. 4a for the electrolyte free and Fig. 4b for the 0.1 M $NaNO_3$ containing sol (in the aqueous part). The first possesses strongly pronounced peaks

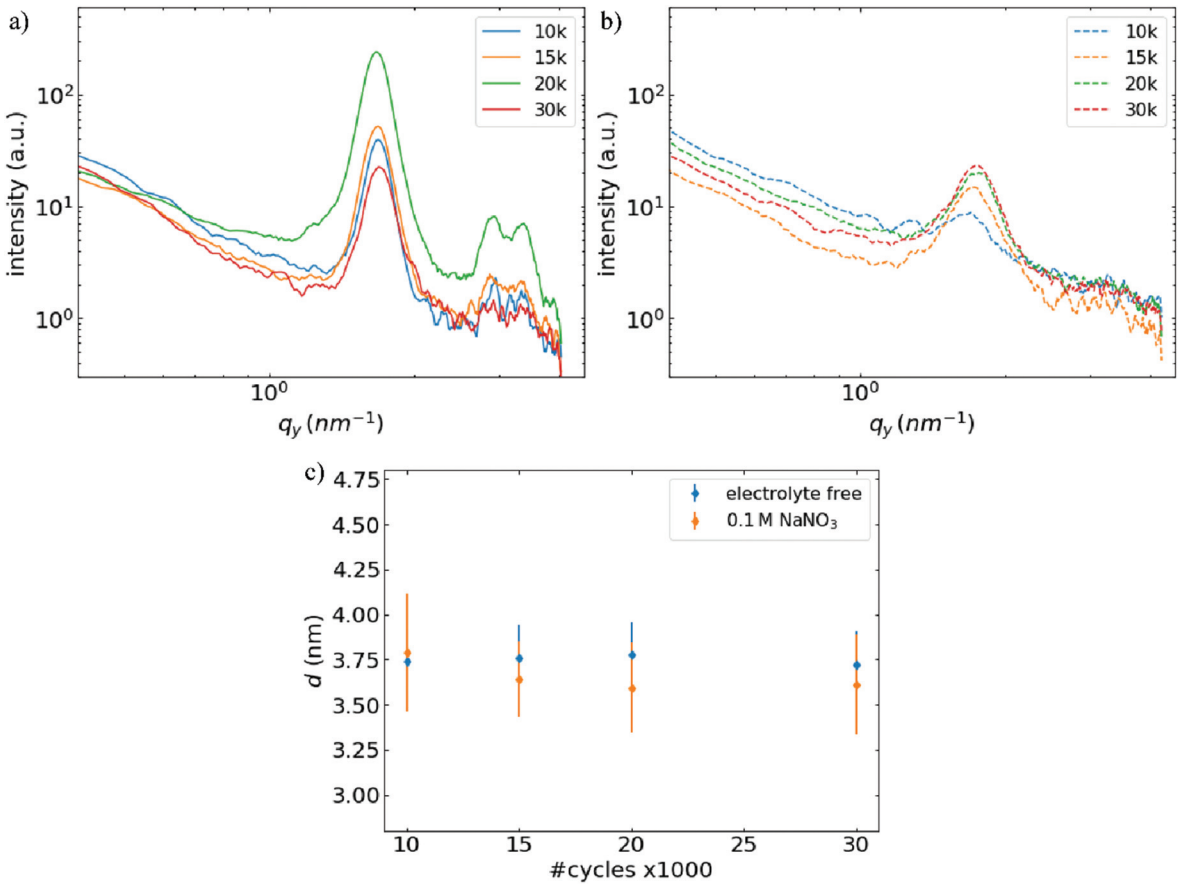

Fig. 4 Horizontal scattering profiles for mesoporous silica films produced at 100 Hz, between −1.0 V and −2.0 V with (a) electrolyte-free and (b) 0.1 M $NaNO_3$ containing sol. (c) Comparison of the *d*-spacings corresponding to the peaks shown in (a) and (b) calculated using $d = 2\pi/q$.

of up to second order, while the latter only has a first order peak. This shows that the structure is hexagonal (peaks at 1, $\sqrt{3}$ and 2 times q_0, values for 10 000, 20 000 and 30 000 periods shown in Table S2†),[30] and that the films made using the nitrate-free sol have a higher degree of ordering than the ones using the conventional sol. From each q_0, the distance between the vertically aligned pores can be calculated (pore-spacing). This represents a value averaged over the entire sample length (0.3 mm × 15 mm). Fig. 4c displays a comparison of the pore-spacing (denoted as d) corresponding to the peaks shown in Fig. 4a and b ($d = 2\pi/q_0$). The blue dots corresponding to the nitrate-free sol show a very consistent value of roughly 3.75 nm, while the distances using the conventional sol (orange) appear to slightly decrease with increasing number of AC periods. This is probably a result of the increased peak width of those points, as the data is still in overall agreement for both conditions within their error bars. The peak width here can be interpreted as the uncertainty of the pore spacing along the probed area of the film. The increased value could be explained as the result of the strong contribution of particle aggregates to the scattering signal, resulting in the ring feature overlaying the horizontal spots. In addition, the enhanced generation of hydroxide due to the presence of $NaNO_3$ in the sol could disturb the self-assembly process during film formation.

The diminished occurrence of particle aggregates through the use of the sinusoidal potential can be explained as follows: as calculated by Liu *et al.*, the deposition process involves a minimum time, t_F, which is needed in order to reach a state at which homogeneous gelation (aggregate formation) occurs.[31] For galvanostatic conditions, this time has been found to lie in the range of seconds (2–3 s). Prior to that time, heterogenous gelation (film formation) occurs if a critical concentration of reactive species has been reached, which therefore represents the lower time limit. One can hence conclude that the pulsing of hydroxide ion flux and lower overall flux achieved with sinusoidal potential leads to the effective reaction time staying below t_F, favouring the deposition of the compact film instead of particle aggregates. This perspective can also be applied to the previously mentioned publication[18] on the use of a rotating disk electrode to this effect, where the species are continuously flushed past the electrode and hence never reach the critical time of homogeneous condensation.

To further test this hypothesis, additional experiments were carried out using the previously used nitrate-free sol, where the frequency of the sinusoidal potential was set to 0.1, 1, 10,

20, 50, 200, 300, 400 and 500 Hz. The number of periods was adapted so that every deposition would be done for a fixed time of 100 s overall, as this corresponds to the sample deposited at 100 Hz for 10 000 periods with minimal aggregates observed. Fig. S5† shows the corresponding SEM data, which clearly visualises the increased number of particle aggregates for frequencies below 20 Hz. When increasing the frequency from there onwards, their number seems to further decrease slightly, with very little change noticeable for frequencies between 300 and 500 Hz. The maximum frequency used here represents the limit of the available potentiostat. This coincides with the magnitude of current obtained after filtering out the respective driving frequencies, as shown in Fig. S6.† It decreases (becoming more positive) with increasing frequency, although one must note the strong oscillations still present at 0.1 Hz even after filtering out this frequency. Beyond 20 Hz, the current profiles converge at roughly −0.12 mA, but the higher frequencies still seem to possess slightly more positive values. GISAXS measurements (Fig. S7†) of the samples confirm the successful generation of vertically structured silica films for all frequencies (spots in horizontal direction), as well as the increased number of particle aggregates at lower frequencies indicated by the ring signal in Fig. S7(a–c).† Selected cross-sections of the samples (see Fig. S8†) show that the use of higher frequencies (>100 Hz) generates compact films (Fig. S8b and c†) while the one at 20 Hz seems to be rather patchy and inconsistent in its thickness. These results allow for the conclusion that higher deposition frequencies lead to fewer particle aggregates. Lowering the frequency makes samples resemble those obtained at constant potential. This validates the previously established hypothesis that the application of a sinusoidal potential diminishes the number of particles and their aggregates during EASA, if the frequency of the signal is sufficiently high to prevent any precursor species not directly in the vicinity of the electrode undergoing condensation.

The films were further characterised through cyclic voltammetry using hexaammineruthenium(III) chloride ($[Ru(NH_3)_6]Cl_3$). Results from measurements at 20 mV s^{-1} are shown for the first cycle in Fig. 5 (additional cycles are shown in Fig. S9†). This cationic probe was chosen because it reliably indicates whether the surfactant was properly removed from the silica film, as it does not penetrate the surfactant within the film.[12] The solid black line in Fig. 5 shows the current response obtained using a blank TiN substrate. The current response through the silica films as prepared is significantly smaller than that with blank TiN, indicating continuous coverage of the electroactive area. After surfactant removal, the redox peaks become visible again, with consistently higher currents recorded compared with the blank substrate. This observation is common for mesoporous silica films, where cationic probes tend to accumulate in the pores due do their negatively charged silica walls.[32] This confirms the successful generation of vertically aligned silica films through the application of a sinusoidal potential.

The resulting structures have dimensions in good agreement with silica films made by applying a constant potential to an electrode situated within a regular silica sol containing

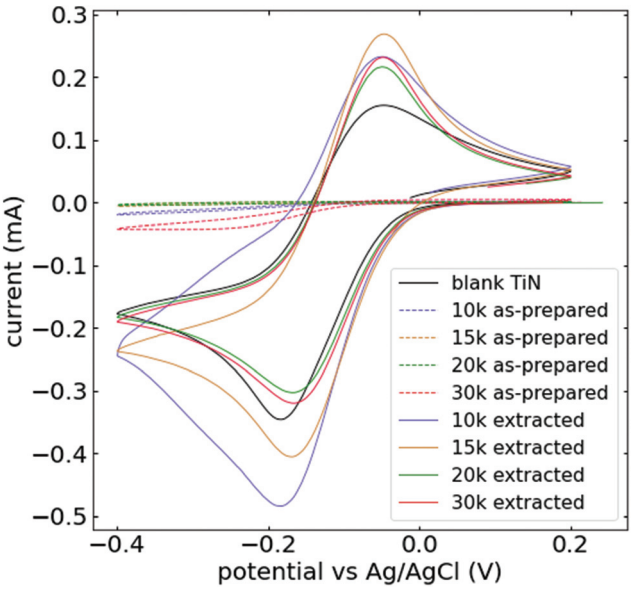

Fig. 5 Cyclic voltammetry of mesoporous silica films (prepared at 100 Hz) on TiN in 5 mM $[Ru(NH_3)_6]Cl_3$ with 0.1 M $NaNO_3$ between −0.4 V and 0.2 V *vs.* Ag/AgCl at a scan rate of 20 mV s^{-1}, one cycle each. Solid black line shows response of a blank TiN substrate with an electrode area of 5 × 15 mm. Coloured dashed lines show the current response before, solid ones after, surfactant removal.

$NaNO_3$. This novel route hence allows for the generation of high-quality silica films with decreased amount of particle aggregates, as required for any application needing a "clean" film surface. Further tuning of the AC protocol and the sol composition might make aggregate-free depositions possible at larger thicknesses, with obtainable films beyond microns in thickness. This could involve the use of an asymmetrical square wave, with the duty cycle being only $1/10^{th}$ of the period to further reduce the flux of hydroxide.

Conclusions

In order to reduce particle growth on the surface of EASA-derived silica films, a new approach using a sinusoidal potential and an electrolyte-free sol composition was tried and tested. The film thickness was 3 times larger than the original protocol using DC conditions. Omission of sodium nitrate in the sol led to a fivefold decrease in the number of aggregated particles when using an oscillating potential. This is a result of improved diffusion control of the hydroxide species away from the electrode, slowing down particle formation in the bulk solution. The films exhibited a high level of ordering of the vertically oriented pores.

Experimental

A standard three-electrode setup was used, consisting of TiN working, Pt gauze counter and Ag/AgCl wire as pseudo refer-

ence electrodes. TiN substrates were prepared by sputtering 200 nm of TiN onto a 700 μm thick silicon wafer (Buehler Helios, rate: 0.135 nm s^{-1}), which results in surfaces with a roughness of 1 nm (H = 0.349, lateral correlation length = 20.72 nm). The nitrate-free silica sol was prepared in a mixture of 20 ml of deionised water (Suez) and 20 ml of ethanol (Fisher Scientific). The pH was adjusted to 3 (Mettler Toledo five-easy) using 0.24 M HCl (Fisher Scientific). Cetyltrimethylammonium bromide (480 mg $[Me_3NC_{16}H_{33}]Br$; Sigma Aldrich) was added under heavy stirring until fully dissolved. Tetraethyl orthosilicate (905 μL, Sigma Aldrich) was added under slow stirring and the sol was left to hydrolyse for 1 h. Straight after that, depositions were carried out using a potentiostat (Biologic SP-150). The applied potential was a sinusoidal signal with a frequency ranging from 0.1–500 Hz between −1.0 V and −2.0 V *vs.* Ag/AgCl reference electrode. 100 Hz was subsequently selected as optimised frequency for silica films deposition. The electrode area was limited to 5 × 15 mm using nail polish to mask off the remaining part of the substrate. Deposition time was given by the number of periods, of which 10 000 were the initial smallest number at which a proper film could be seen on the TiN substrate. Deposition was hence done for 10 000, 15 000, 20 000 and 30 000 periods respectively after which the samples were immediately rinsed with water.

Hexaammineruthenium chloride ($[Ru(NH_3)_6]Cl_3$) was used in cyclic voltammetry experiments on the newly generated silica films. Measurements were performed for each sample both before and after removal of the surfactant through immersion in 0.2 M HCl in ethanol overnight. The potential was scanned between −0.4 V and 0.2 V *vs.* Ag/AgCl in an aqueous solution containing 5 mM $[Ru(NH_3)_6]Cl_3$ with 0.1 M $NaNO_3$ using a Pt gauze as counter electrode.

GISAXS experiments were carried out on a Rigaku Smartlab diffractometer with a HiPix 2D detector and Cu-K_α radiation. The sample-detector distance was 301 mm, the collimator size was 300 μm and the exposure time was 15 min. SEM images were recorded with a Zeiss Gemini or Jeol JSM 6500F and 7200F. ImageJ[33] was used to measure the film thickness of the porous films from their cross sections.

Conflicts of interest

There are no conflicts to declare.

Acknowledgements

This work has been supported by EPSRC through the Advanced Devices by Electroplating program grant (ADEPT; EP/N035437/1) and through equipment funding (EP/K00509X/1 and EP/K009877/1). All data supporting this study are openly available from the University of Southampton repository at **https://doi.org/10.5258/SOTON/D2119**.

Notes and references

1 L. Nicole, C. Boissière, D. Grosso, A. Quach and C. Sanchez, *J. Mater. Chem.*, 2005, **15**, 3598–3627.
2 K. Domansky, J. Liu, L. Q. Wang, M. H. Engelhard and S. Baskaran, *J. Mater. Res.*, 2001, **16**, 2810–2816.
3 A. Palaniappan, X. Su and F. E. H. Tay, *J. Electroceram.*, 2006, **16**, 503–505.
4 N. Ehlert, P. P. Mueller, M. Stieve, T. Lenarz and P. Behrens, *Chem. Soc. Rev.*, 2013, **42**, 3847–3861.
5 C. J. Brinker, *MRS Bull.*, 2004, **29**, 631–640.
6 Y. Lu, R. Ganguli, C. A. Drewien, M. T. Anderson, C. Jeffrey Brinker, W. Gong, Y. Guo, H. Soyez, B. Dunn, M. H. Huang and J. I. Zink, *Nature*, 1997, **389**, 364–368.
7 D. Zhao, P. Yang, N. Melosh, J. Feng, B. F. Chmelka and G. D. Stucky, *Adv. Mater.*, 1998, **10**, 1380–1385.
8 X. Zhang, Y. Dou, C.-Y. Mou, A. M. Asiri, Z. Teng, W. Li, G. Zheng and D. Zhao, *Angew. Chem., Int. Ed.*, 2012, **51**, 2173–2177.
9 G. S. Attard, P. N. Bartlett, N. R. B. Coleman, J. M. Elliott, J. R. Owen and J. H. Wang, *Science*, 1997, **278**, 838–840.
10 C. Li, B. Jiang, N. Miyamoto, J. H. Kim, V. Malgras and Y. Yamauchi, *J. Am. Chem. Soc.*, 2015, **137**, 11558–11561.
11 T. Imokawa, K. J. Williams and G. Denuault, *Anal. Chem.*, 2006, **78**, 265–271.
12 A. Walcarius, E. Sibottier, M. Etienne and J. Ghanbaja, *Nat. Mater.*, 2007, **6**, 602–608.
13 A. Walcarius, J. Ghanbaja, M. Etienne, E. Aubert, C. Lecomte and A. Goux, *Chem. Mater.*, 2009, **21**, 731–741.
14 A. Walcarius, *Chem. Soc. Rev.*, 2013, **42**, 4098–4140.
15 C. Robertson, R. Beanland, S. A. Boden, A. L. Hector, R. J. Kashtiban, J. Sloan, D. C. Smith and A. Walcarius, *Phys. Chem. Chem. Phys.*, 2015, **17**, 4763–4770.
16 C. Robertson, A. W. Lodge, P. Basa, M. Carravetta, A. L. Hector, R. J. Kashtiban, J. Sloan, D. C. Smith, J. Spencer and A. Walcarius, *RSC Adv.*, 2016, **6**, 113432–113441.
17 W. Stöber, A. Fink and E. Bohn, *J. Colloid Interface Sci.*, 1968, **26**, 62–69.
18 G. Vanheusden, H. Philipsen, S. J. F. Herregods and P. M. Vereecken, *Chem. Mater.*, 2021, **33**, 7075–7088.
19 G. Giordano, N. Vilà, E. Aubert, J. Ghanbaja and A. Walcarius, *Electrochim. Acta*, 2017, **237**, 227–236.
20 A. Walcarius, *Acc. Chem. Res.*, 2021, **54**, 3563–3575.
21 N. Ibl, J. C. Puippe and H. Angerer, *Surf. Technol.*, 1978, **6**, 287–300.
22 E. Leontidis, *Curr. Opin. Colloid Interface Sci.*, 2002, **7**, 81–91.
23 S. Che, M. Kaneda, O. Terasaki and T. Tatsumi, in *Studies in Surface Science and Catalysis*, 2003, vol. 146, pp. 431–434.
24 K. C. Kao, C. H. Lin, T. Y. Chen, Y. H. Liu and C. Y. Mou, *J. Am. Chem. Soc.*, 2015, **137**, 3779–3782.
25 S. Besson, T. Gacoin, C. Ricolleau, C. Jacquiod and J. P. Boilot, *J. Mater. Chem.*, 2003, **13**, 404–409.
26 S. Besson, C. Ricolleau, T. Gacoin, C. Jacquiod and J. P. Boilot, *Microporous Mesoporous Mater.*, 2003, **60**, 43–49.
27 B. Platschek, R. Kóhn, M. Dóblinger and T. Bein, *ChemPhysChem*, 2008, **9**, 2059–2067.

28 M. Chen, I. Burgess and J. Lipkowski, *Surf. Sci.*, 2009, **603**, 1878–1891.
29 Y. Guillemin, M. Etienne, E. Sibottier and A. Walcarius, *Chem. Mater.*, 2011, **23**, 5313–5322.
30 S. H. Lim, T. Lee, Y. Oh, T. Narayanan, B. J. Sung and S. M. Choi, *Nat. Commun.*, 2017, **8**, 360.
31 L. Liu and A. Walcarius, *Phys. Chem. Chem. Phys.*, 2017, **19**, 14972–14983.
32 D. Basnig, N. Vilá, G. Herzog and A. Walcarius, *J. Electroanal. Chem.*, 2020, **872**, 113993.
33 M. D. Abràmoff, P. J. Magalhães and S. J. Ram, *Biophotonics Int.*, 2004, **11**, 36–41.